Available online at www.sciencedirect.com
ScienceDirect
Ceramics International 37 (2011) 2981–2989
CERAMICS INTERNATIONAL
www.elsevier.com/locate/ceramint

Synthesis of a TiO_2 ceramic membrane containing $SrCo_{0.8}Fe_{0.2}O_3$ by the sol–gel method with a wet impregnation process for O_2 and N_2 permeation

Abdul Latif Ahmad *, Nur Aimie Abdullah Sani, Sharif Hussein Sharif Zein

School of Chemical Engineering, Universiti Sains Malaysia, Engineering Campus, Seri Ampangan, 14300 Nibong Tebal, Seberang Perai Selatan, Pulau Pinang, Malaysia

Received 24 January 2011; received in revised form 27 March 2011; accepted 27 March 2011
Available online 6 April 2011

Abstract

A $SrCo_{0.8}Fe_{0.2}O_3$ impregnated TiO_2 membrane (TiO_2–$SrCo_{0.8}Fe_{0.2}O_3$ membrane) was successfully prepared using a sol–gel method in combination with a wet impregnation process. The membrane was subjected to a single gas permeance test using oxygen (O_2) and nitrogen (N_2). The TiO_2 membrane was immersed in the $SrCo_{0.8}Fe_{0.2}O_3$ solution, dried and then calcined to affix $SrCo_{0.8}Fe_{0.2}O_3$ into the membrane. The effect of the acid/alkoxide (H^+/Ti^{4+}) molar ratio of the TiO_2 sol on the TiO_2 phase transformation was investigated. The optimal molar ratio was found to be 0.5, which resulted in nanoparticles with a mean size of 5.30 nm after calcination at 400 °C. The effect of calcination temperature on the phase transformation of TiO_2 and $SrCo_{0.8}Fe_{0.2}O_3$ was investigated by varying the calcination temperature from 300 to 500 °C. X-ray diffraction spectroscopy (XRD) and Fourier transform infrared (FTIR) analysis confirmed that a calcination temperature of 400 °C was preferable for preparing a TiO_2–$SrCo_{0.8}Fe_{0.2}O_3$ membrane with fully crystallized anatase and $SrCo_{0.8}Fe_{0.2}O_3$ phases. The results also showed that polyvinyl alcohol (PVA) and hydroxypropyl cellulose (HPC) were completely removed. Field emission scanning electron microscopy (FESEM) analysis results showed that a crack-free and relatively dense TiO_2 membrane (~0.75 μm thickness) was created with a multiple dip-coating process and calcination at 400 °C. The gas permeation results show that the TiO_2 and TiO_2–$SrCo_{0.8}Fe_{0.2}O_3$ membranes exhibited high permeances. The TiO_2–$SrCo_{0.8}Fe_{0.2}O_3$ membrane developed provided greater O_2/N_2 selectivity compared to the TiO_2 membrane alone.

Keywords: D. Perovskites; TiO_2 ceramic membrane; Sol–gel method; O_2 and N_2 permeation

1. Introduction

Ceramic membranes offer many advantages over polymeric membranes. They are stable at high temperatures, exhibit good chemical stability (especially in organic solvents) and have a high pressure resistance [1]. Ceramic membranes are superior for applications in gas separation, food and biotechnology, as well as in the filtration and treatment of water and waste water [2]. The ceramics that have been most extensively studied for membrane applications include Al_2O_3, TiO_2, ZrO_2 and SiO_2. TiO_2 membranes have garnered considerable attention due to their high hydrothermal and chemical stability; good anti-fouling properties [3]; high surface reactivity to gases, which makes it suitable as a catalyst [4] and high specific surface area for gas sensors [5]. Their potential applications include ultrafiltration processes, catalytic/photocatalytic membrane reactors, gas separations/reactions and gas sensing [6].

TiO_2 exists in a number of crystalline forms, the most important of which are anatase, rutile and brookite. Anatase and rutile are both tetragonal in structure, while brookite has an orthorhombic structure [7]. Anatase is the thermodynamically metastable form with respect to rutile, under all conditions of temperature and pressure [8]. The volume free energy of the rutile phase is always lower than that of the anatase phase. Therefore, heat treatment transforms the anatase phase to the stable rutile phase. The temperature of the transformation depends heavily on the nature and structure of the precursor and on the preparation conditions. Most of the chemical preparation methods yield TiO_2 in the metastable anatase phase and shift it to the rutile phase after further heat treatment [9,10].

The perovskite-type oxide, $SrCo_{0.8}Fe_{0.2}O_3$, is a typical mixed ionic electronic conducting membrane material that has

* Corresponding author. Tel.: +60 4 593 7788x6414; fax: +60 4 594 1013.
E-mail address: chlatif@eng.usm.my (A.L. Ahmad).

0272-8842/$36.00 © 2011 Published by Elsevier Ltd and Techna Group S.r.l.
doi:10.1016/j.ceramint.2011.03.036

drawn a significant amount of attention and has been applied in the chemical and petroleum industries. Presently, the use of $SrCo_{0.8}Fe_{0.2}O_3$ as an O_2 separation membrane has been considered because of its higher oxygen ion and electron conductivity. $SrCo_{0.8}Fe_{0.2}O_3$ can also operate steadily for longer durations at high temperatures [11]. A $SrCo_{0.8}Fe_{0.2}O_3$ membrane is usually used alone and is prepared using a conventional solid state method to form a $SrCo_{0.8}Fe_{0.2}O_3$ powder. This powder is compressed into a disc and sintered before application in gas-separation processes [12].

To the best of our knowledge, there are no reports on the preparation of TiO_2 membranes containing $SrCo_{0.8}Fe_{0.2}O_3$, especially using the sol–gel method in combination with a wet impregnation process. Therefore, this paper reports the synthesis of TiO_2–$SrCo_{0.8}Fe_{0.2}O_3$ membranes for O_2 and N_2 permeances. The TiO_2 membrane was prepared by a sol–gel method and $SrCo_{0.8}Fe_{0.2}O_3$ was affixed to the TiO_2 membrane using a wet impregnation process. The membranes were characterized using transmission electron microscopy (TEM), XRD, FESEM and FTIR. The membrane developed was tested on O_2 and N_2 gases and the O_2/N_2 selectivity across the TiO_2 and TiO_2–$SrCo_{0.8}Fe_{0.2}O_3$ were documented.

2. Methodology

2.1. Preparation of membrane support and binders

A porous TiO_2 disc (prepared from titanium (IV) oxide powder) was used as a membrane support for a TiO_2–$SrCo_{0.8}Fe_{0.2}O_3$ membrane. The support had a 20-mm diameter and 2-mm thickness. About 1.75 g of TiO_2 powder was loaded into the stainless steel mold. The mold was then pressed using hydraulic press equipment up to 20 MPa pressure. After pressing, the support was dried at 70 °C, followed by a calcination process at 965 °C for 4 h. To prevent cracking of the support surface, the heating and cooling rate employed during the calcinations was 2 °C/min.

Polyvinyl alcohol (PVA) and hydroxypropyl cellulose (HPC) were used as binders to prevent the formation of cracks on the thin membrane surface. They were also used to affix the TiO_2–$SrCo_{0.8}Fe_{0.2}O_3$ membrane to the membrane support. The PVA solution was prepared by dissolving 0.1 g of PVA into 100 ml distilled water, followed by stirring for approximately 1 h. The HPC solution was prepared by dissolving 0.7 g HPC into 100 ml distilled water and stirring for 1 h.

2.2. Preparation of TiO_2 sol

The sol–gel method was used to prepare the TiO_2 sol. The starting materials for the preparation of the TiO_2 sol were the following: (1) titanium tetraisopropoxide (TTIP) as the TiO_2 precursor, (2) nitric acid as the catalyst for the peptization, (3) distilled water as the dispersing medium and (4) isopropanol as the solvent. TiO_2 sol was prepared by hydrolysis of TTIP. A solution of TTIP in isopropanol (0.45 M) was added drop wise into a solution of isopropanol (4.5 M) in distilled water under vigorous stirring. After the hydrolysis reaction was complete, the remaining white precipitate of titanium hydroxide ($Ti(OH)_4$) was filtered and washed with water to remove the alcohol. The filtrate was then dispersed in distilled water (Ti^{4+}) and nitric acid was added to achieve a 0.5 molar ratio of acid/alkoxide (H^+/Ti^{4+}). The process was repeated with the following ratios: 0.5, 1.5, 2.5 and 3.5. Next, the solution was peptized for 2 h at 70 °C. A closed beaker was used to enhance the rate of peptization. To break the weak bonds of the agglomerated particles, the sol was treated ultrasonically for 30 min. The final product was a blue, semi-opaque colloidal dispersion at a concentration of 0.325 M. A dilute concentration of the dispersion was produced by dilution with distilled water.

2.3. Preparation of the $SrCo_{0.8}Fe_{0.2}O_3$ solution

$SrCo_{0.8}Fe_{0.2}O_3$ was prepared as described in a previous publication [13]. $Sr(NO_3)_2$, $Co(NO_3)_2{\cdot}6H_2O$ and $FeCI_3{\cdot}6H_2O$ were weighed in equimolar amounts and dissolved in distilled water (0.7 M). The solution was stirred for approximately 1 h to ensure that it was completely dissolved. The $SrCo_{0.8}Fe_{0.2}O_3$ phase was obtained after the membrane was calcined.

2.4. Preparation of the TiO_2–$SrCo_{0.8}Fe_{0.2}O_3$ membrane

The TiO_2 membrane was created from the TiO_2 sol. The $SrCo_{0.8}Fe_{0.2}O_3$ was then affixed within the TiO_2 membrane pores using a wet impregnation process.

The dipping solution for the TiO_2 membrane contained 30 mL 0.05 M TiO_2 sol mixed with 10 mL PVA solution and 20 mL HPC solution. An adequate amount of dipping solution was used to coat the membrane support by dip-coating to form the supported TiO_2 membranes. The membranes were then dried and calcined at different temperatures (100, 300 and 400 °C) for 2 h. The membranes were screened using TEM and FTIR analysis and evaluated for membrane performance.

For the $SrCo_{0.8}Fe_{0.2}O_3$ impregnation process, the TiO_2 membrane was immersed in a $SrCo_{0.8}Fe_{0.2}O_3$ solution for 10 min. The membrane was then dried and calcined under atmospheric air at 400 °C for 4 h. The TiO_2–$SrCo_{0.8}Fe_{0.2}O_3$ membrane was tested using XRD and FESEM analyses and evaluation of membrane performance was conducted.

2.5. Membrane characterization

TEM (Philips CM12) was performed to investigate the dispersion of the particles in the TiO_2 sol. The phase transformation of the membrane during the calcination process was identified using XRD (Philips PW1729 X-ray generator with Philips PW1820 diffractometer) with Cu Kα radiation. The surface and thickness of the membrane were observed using FESEM (Leo Supra 50VP). FTIR analysis was performed using the FTIR 2000 Perkin Elmer spectrophotometer and the samples were prepared using a KBr pellet.

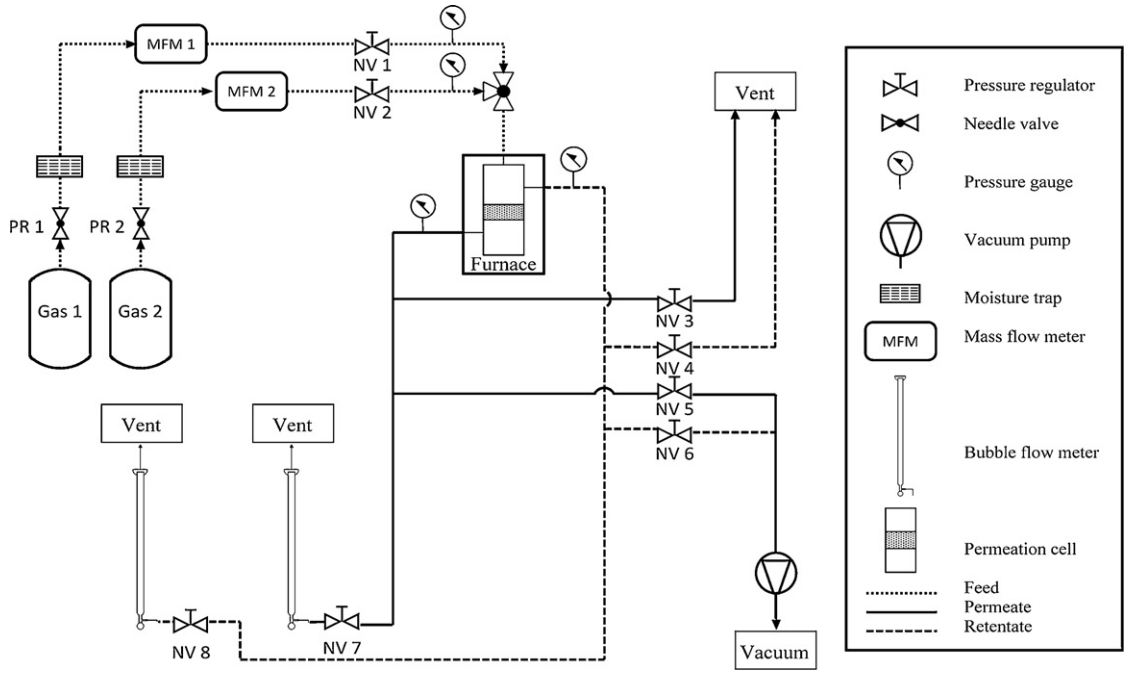

Fig. 1. Schematic diagram of the membrane gas permeation test rig.

2.6. Gas permeation measurement

The experimental apparatus utilized for the gas permeation measurements is illustrated in Fig. 1. Single-gas permeance was determined for O_2 and N_2, and the ideal selectivity was defined as the ratio of their permeances. The permeance of the membrane (K) in mol/m^2 Pa s was obtained using Eq. (1) [14]:

$$K = \frac{q_p}{A_m \Delta P} \quad (1)$$

where q_p is the gas flow rate of the permeate stream, A_m is the membrane's effective surface area and ΔP is the pressure difference between the feed and permeate streams. The ideal selectivity of the membrane,$\alpha O_z/N_z$, is equal to the ratio of permeances between O_2 and N_2, as shown in Eq. (2) [14]:

$$\alpha_{O_z/N_z} = \frac{K_{O_2}}{K_{N_2}} \quad (2)$$

The permeance of the individual gases was determined in the temperature range of 28–350 °C and at a fixed operating pressure of 3 bars.

3. Results and discussion

3.1. Effect of the H^+/Ti^{4+} molar ratio on the TiO_2 phase transformation

In this study, nitric acid was used as the peptizing agent. The TiO_2 membrane properties were studied at several H^+/Ti^{4+} molar ratios, ranging from 0.5 to 3.5. This study was conducted in the absence of PVA and HPC. Fig. 2(a)–(d) shows the TEM images of the TiO_2 membrane after calcination at 400 °C at different H^+/Ti^{4+} molar ratios. The TiO_2 sol created at a 0.5 molar ratio had the smallest-sized nanoparticles, of roughly spherical shapes (Fig. 2(a)) and a mean size of 5.30 nm, which is in contrast to the result reported by Zaspalis et al. [15] using the same general method (30 nm). Similar trends were reported by Gestel et al. [3] and Alem et al. [16]. However, the nanoparticle size in the TiO_2 sol increased as the H^+/Ti^{4+} molar ratio increased from 0.5 to 3.5, while this increase in molar ratio decreased the pH value from 1.3 to 0.3 (Table 1). A decrease in pH is believed to favor anatase over rutile transformation [17].

During the peptization process, H^+ ions from the nitric acid are adsorbed by the surface of the sol particles. The ions repel each other to form a stable colloidal sol. This electrostatic repulsion also prevents particles from sticking together and forming aggregates [18]. Peptization with acid leads to the breakup of large aggregates into nanoparticles by the electrostatic repulsion of the charged particles. Nanoparticle sols produced gels with efficient particle packing, while aggregated sols produced gels with a much more open structure, higher porosity and a larger pore size. The anatase phase has been found to have an isoelectric point (pH_{iep}) that ranges from 4.7 to 6.7. At a pH well below the pH_{iep} (e.g., pH = 1–2), the surface of TiO_2 would have a net positive charge, yielding nanoparticle sol [7]. Formation of small pore size and crack-free membrane heavily depends on the condition of the utilized sol. It has been shown that membranes with a smaller pore diameter and a narrower pore size distribution can be made from a sol of nanoparticles [19].

Fig. 3 shows the XRD patterns of the TiO_2 membrane with different H^+/Ti^{4+} molar ratios and a calcination temperature of 400 °C. The findings indicate that the TiO_2 sol with a 0.5 molar ratio exhibits an amorphous anatase phase as the dominant XRD peak at $2\theta = 25.3°$, whereas an increased molar ratio of TiO_2 sol shows a partial rutile phase transformation. The

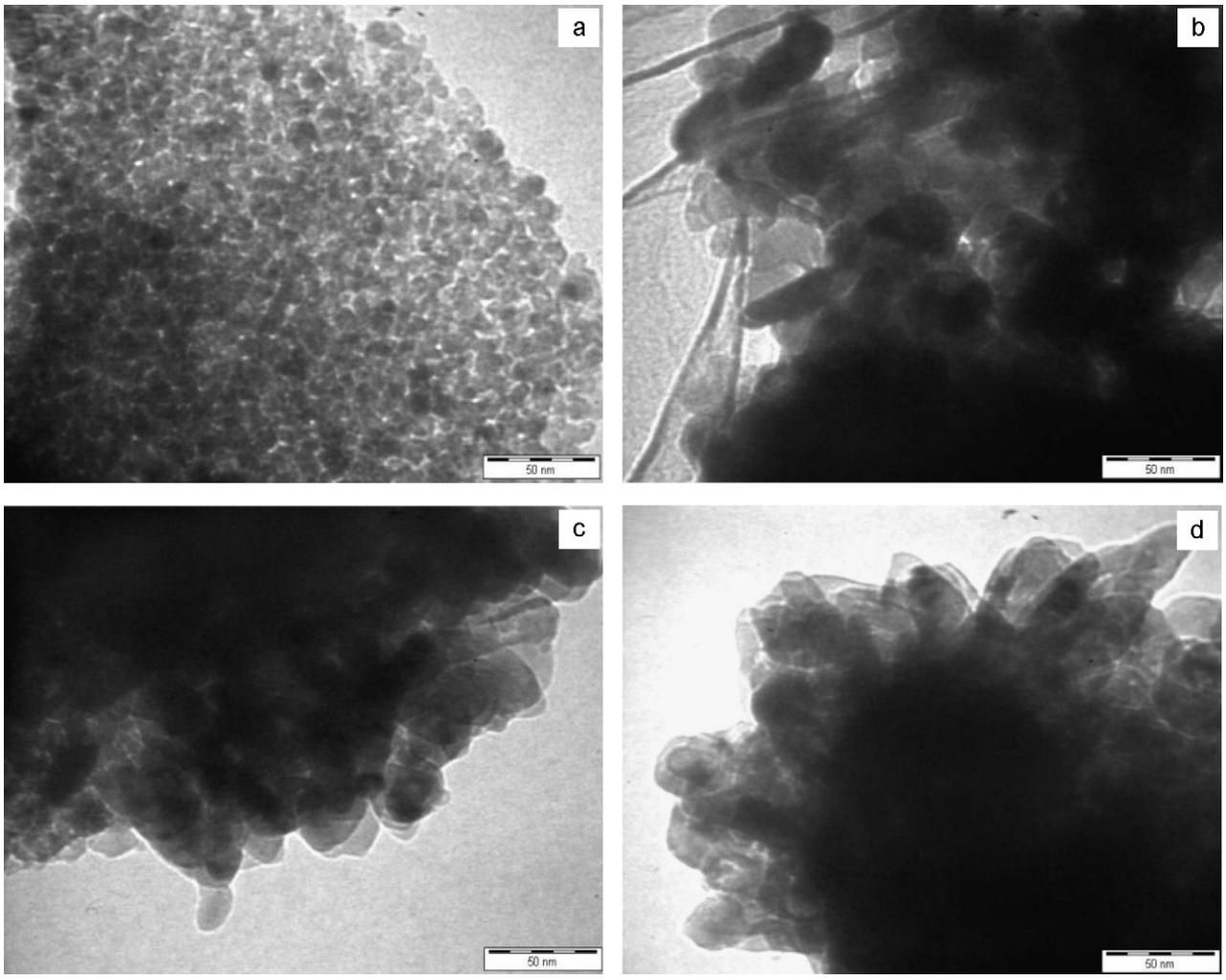

Fig. 2. TEM image of TiO_2 particles after calcination at 400 °C at different H^+/Ti^{4+} molar ratios: (a) 0.5, (b) 1.5, (c) 2.5 and (d) 3.5.

addition of acid has a strong influence on the crystal structure of TiO_2. The XRD pattern of TiO_2 sol at a 3.5 molar ratio illustrates an anatase phase that has fully transformed into a rutile phase, with dominant XRD peaks at $2\theta = 27.4°$ and 54.0°. The anatase–rutile phase transformation was accelerated by increasing the acid concentration. This result was confirmed by a TEM image showing nanoparticle of increased size, indicating that phase transformation occurs at an anatase phase with a smaller nanoparticle size rather than in the rutile phase.

Thus, based upon the TEM and XRD observations, the optimal H^+/Ti^{4+} molar ratio was found to be 0.5, with a 2 h peptization process at 70 °C. These conditions were sufficient to yield a blue (semi-opaque) colloidal dispersion as the final product with a predominantly anatase phase.

Table 1
pH value of TiO_2 sol at different H^+/Ti^{4+} molar ratios.

H^+/Ti^{4+} molar ratio	pH
0.5	1.3
1.5	0.8
2.5	0.4
3.5	0.3

3.2. Effect of calcination temperature on TiO_2 membrane

The bond configurations of TiO_2 membranes calcined at 100, 300 and 400 °C were evaluated by FTIR analysis at wave numbers ranging from 500 to 4000 cm^{-1} (Fig. 4). For the

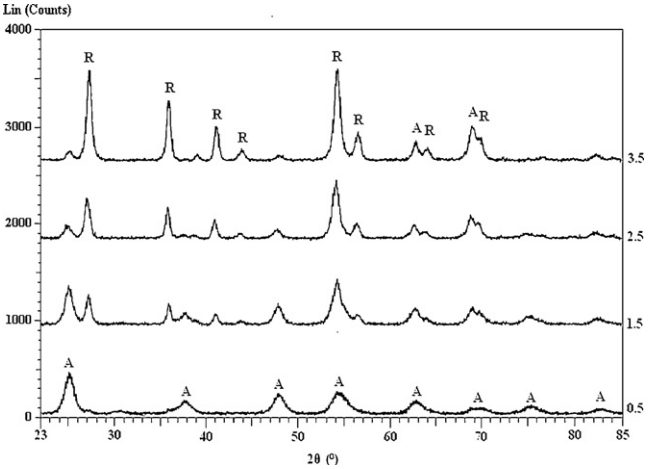

Fig. 3. XRD patterns of TiO_2 membranes calcined at 400 °C at different H^+/Ti^{4+} molar ratios.

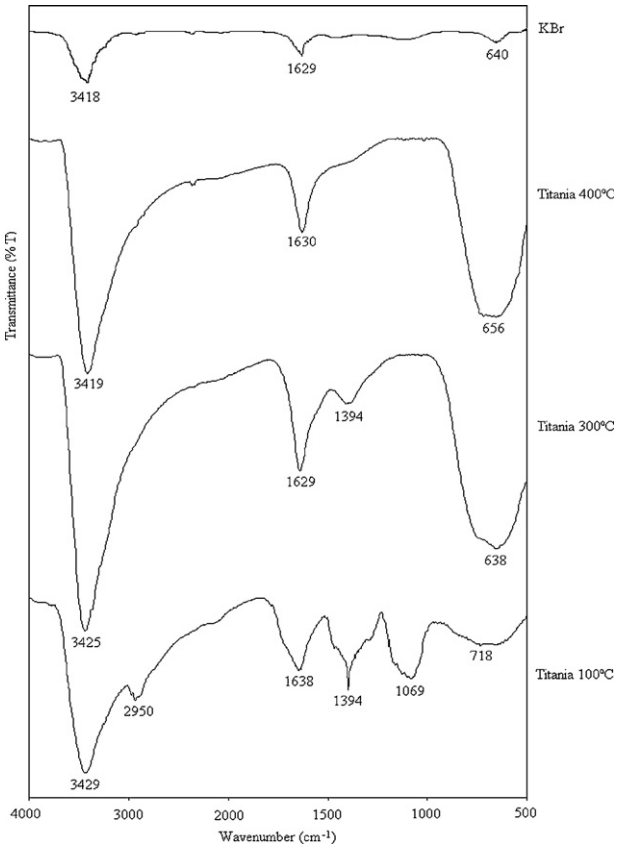

Fig. 4. FTIR spectra of TiO_2 membranes.

membrane calcined at 100 °C, the absorption peak at 3429 cm^{-1} indicates the presence of –OH groups, probably belonging to the Ti–OH bonds and the water absorbed by the membrane. The absorption peak of the –OR group of titanium tetraisopropoxide (TTIP), which was the precursor of the TiO_2 sols, appears at approximately 1069 cm^{-1}. As the calcination temperature was increased above 300 °C, no absorption peak was detected, implying that the four –OR groups of TTIP were substituted with –OH groups of water. As expected, a full conversion of TTIP was obtained by the hydrolysis reaction, resulting in the formation of TiO_2 particles.

The presence of amorphous TiO_2 was clearly noted by the absorption peak at 718 cm^{-1} for the TiO_2 membrane calcined at 100 °C. As the calcination temperature increased, the peak shifted to 638–656 cm^{-1}, corresponding to the Ti–O stretching vibration of TiO_2 in the anatase phase. This result is similar to previous reports [20,21].

The absorption peak at 1394 cm^{-1} for the TiO_2 membranes calcined at 100 °C and 200 °C corresponds to the nitrate (NO_3?) group derived from nitric acid. The absorption peak at 2950 cm^{-1} for the TiO_2 membrane calcined at 100 °C corresponds to the –CH vibrations associated with the vinyl compounds ($-CH{=}CH_2$) derived from PVA and HPC. All of these features gradually vanished with increasing calcination temperature. This effect was attributed to the oxidation of PVA and HPC due to the heat treatment. The absorption peaks at 3418–3429 cm^{-1} and 1629–1638 cm^{-1} that appeared for the TiO_2 membranes calcined at 100, 300 and 400 °C indicate the presence of –OH groups that belong to the adsorbed water in the KBr pellet.

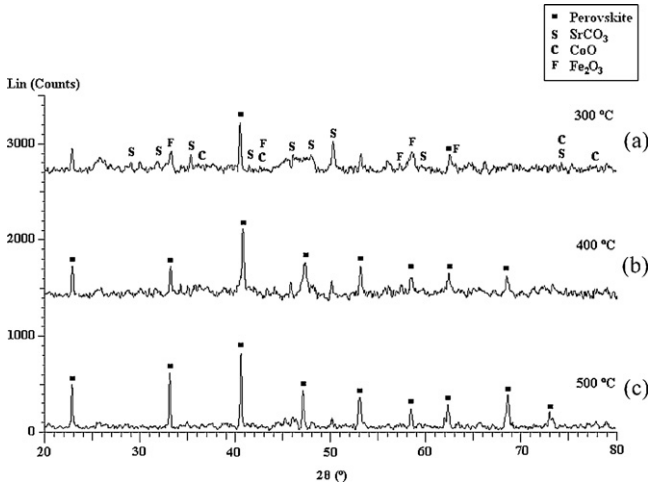

Fig. 5. XRD patterns of $SrCo_{0.8}Fe_{0.2}O_3$ calcined at (a) 300, (b) 400 and (c) 500 °C.

3.3. Effect of calcination temperature on the phase structure of $SrCo_{0.8}Fe_{0.2}O_3$

Fig. 5(a–c) shows the XRD patterns of $SrCo_{0.8}Fe_{0.2}O_3$ calcined at 300, 400 and 500 °C, respectively. The $SrCo_{0.8}Fe_{0.2}O_3$ calcined at 300 °C (Fig. 5(a)) consists of strontium carbonate ($SrCO_3$), iron oxide (Fe_2O_3) and cobalt oxide (CoO).

To prepare the $SrCo_{0.8}Fe_{0.2}O_3$, it needed to be calcined until the proper phase was fully achieved. The observations at Fig. 5(a) result from the incomplete oxidation of $SrCo_{0.8}Fe_{0.2}O_3$. Fig. 5(b and c) shows the phase transformation of $SrCo_{0.8}Fe_{0.2}O_3$ occurred, as indicated by the dominant XRD peak at $2\theta = 40.7°$. Based on the experimental results, the $SrCo_{0.8}Fe_{0.2}O_3$ structure was readily formed at 400 °C. This finding is consistent with previous reports, where a low temperature perovskite-type $CdTiO_3$ membrane was prepared [22]. Therefore, 400 °C was chosen as the $SrCo_{0.8}Fe_{0.2}O_3$ calcination temperature for the TiO_2 membrane to inhibit the anatase–rutile phase transformation.

3.4. Microstructure

An FESEM image of a single coating of a TiO_2 membrane on a membrane support is shown in Fig. 6(a). The TiO_2 membrane was formed on the surface of the support, with some regions remaining uncoated. Cracks were found on the surface of the TiO_2 membrane due to the drying and calcination processes, which removed the water inside the TiO_2 membrane. The release of the water vapor and the shrinkage of the membrane during calcination led to cracks. Fig. 6(b) shows the surface irregularities on the support surface; the thickness of the membrane was estimated to be approximately 0.40 μm. These irregularities are due to the quality of the surface on which the membrane formed. The uneven support surface transfers its roughness to the membrane layers. This roughness is an extra

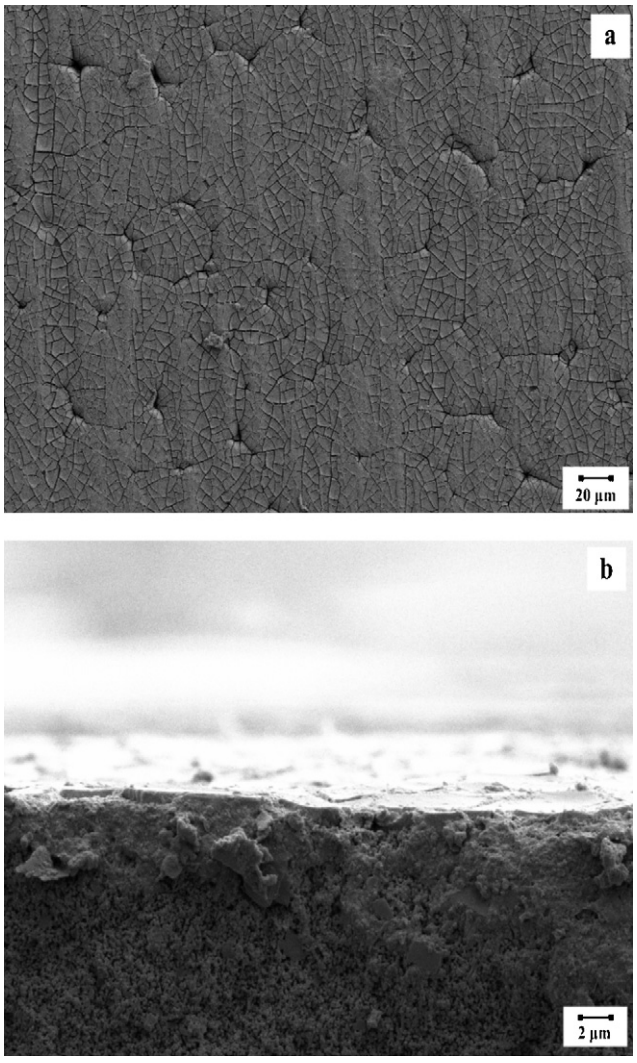

Fig. 6. FESEM images of the TiO_2 membrane (a) surface and (b) cross-sectional area calcined at 400 °C after a first time dip-coating process.

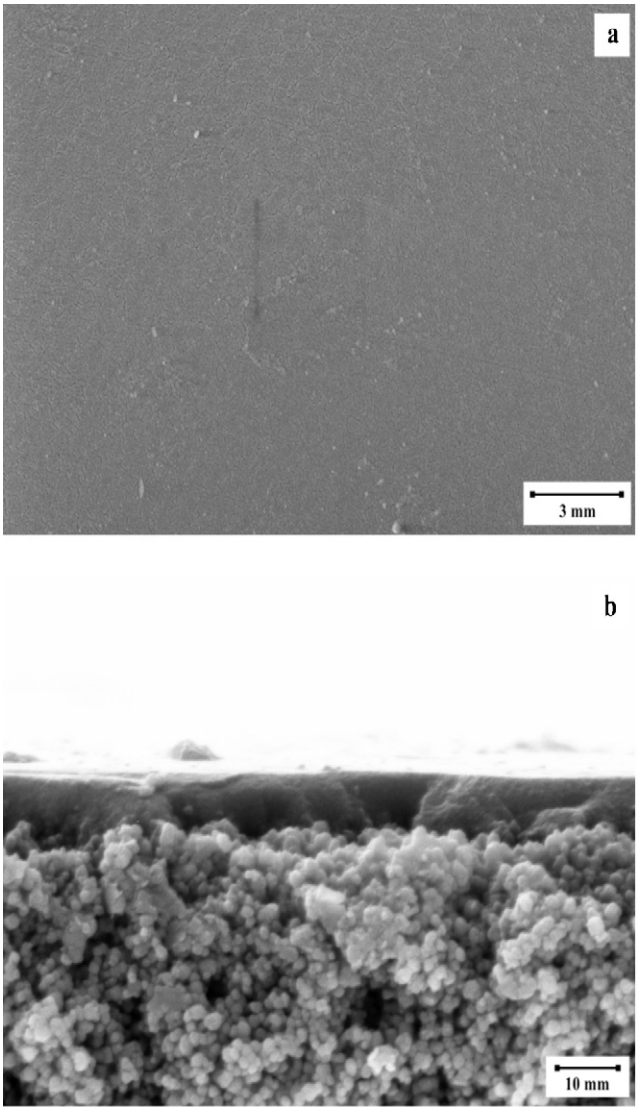

Fig. 7. FESEM images of the TiO_2 membrane (a) surface and (b) cross-section area calcined at 400 °C after five dip-coating processes.

stress-generating factor that might promote nucleation of cracks and could result in a defective membrane [15].

Fig. 7(a) and (b) shows FESEM images of the surface and cross-section, respectively, of the TiO_2 membrane after five dip-coating processes. The surface of the TiO_2 membrane after five coatings became relatively denser and created a more completely coated membrane compared to after a single coating (Fig. 6(a)). Continuous contact exists in the interface, and the thickness of the membrane was found to be approximately 0.75 μm, as shown in Fig. 7(b). This multiple coating technique can reduce the pore size and coat the entire surface of the porous membrane support. After a crack-free TiO_2 membrane was obtained, the $SrCo_{0.8}Fe_{0.2}O_3$ wet impregnation process was performed.

Fig. 8 shows an image of the TiO_2–$SrCo_{0.8}Fe_{0.2}O_3$ membrane, which confirmed the presence of $SrCo_{0.8}Fe_{0.2}O_3$ in the TiO_2 membrane. The surface area of the membrane showed a homogeneous dispersion of $SrCo_{0.8}Fe_{0.2}O_3$ particles on the TiO_2 membrane without cracking.

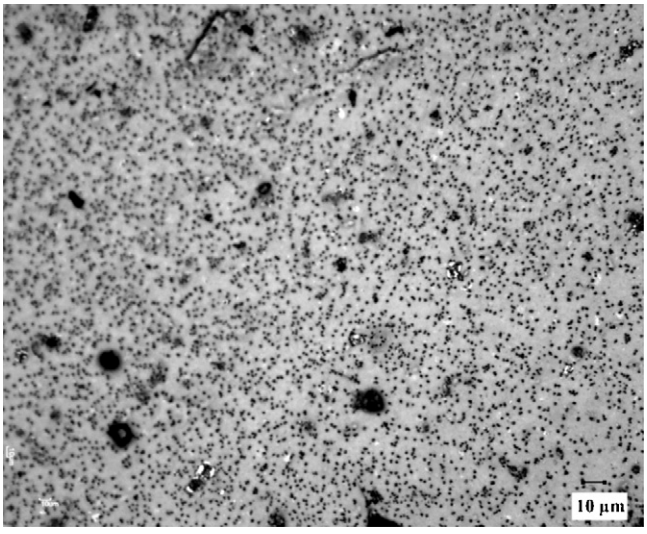

Fig. 8. FESEM image of a TiO_2–$SrCo_{0.8}Fe_{0.2}O_3$ membrane calcined at 400 °C.

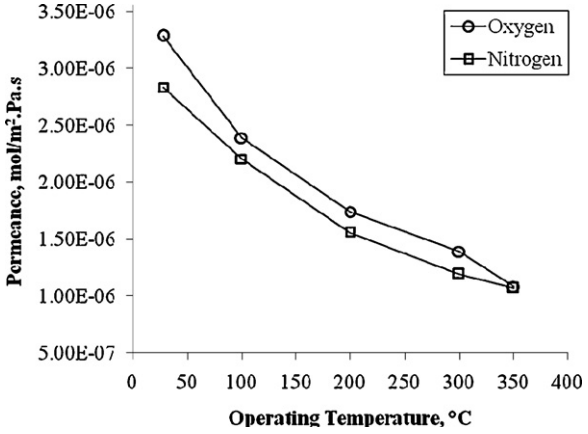

Fig. 9. Permeance of O_2 and N_2 across TiO_2 membrane as a function of the operating temperature.

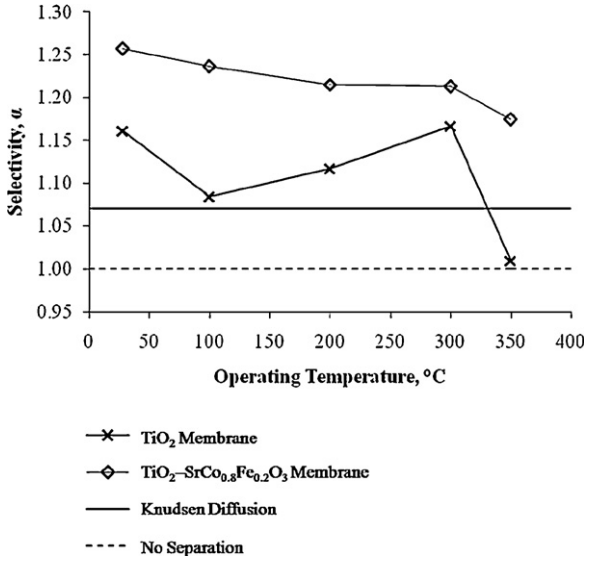

Fig. 11. O_2/N_2 selectivity of the TiO_2 and TiO_2–$SrCo_{0.8}Fe_{0.2}O_3$ membranes as a function of the operating temperature.

3.5. Gas permeation of TiO_2–$SrCo_{0.8}Fe_{0.2}O_3$ membrane

Although TiO_2 membranes offer numerous applications and advantages, they possess selectivity drawbacks. A TiO_2 membrane not only has a high permeance, but also has a low selectivity. In this work, the selectivity of TiO_2 membranes was improved by doping $SrCo_{0.8}Fe_{0.2}O_3$ on the surface of the TiO_2 membrane.

The influence of the operating temperature on the O_2 and N_2 permeances across TiO_2 and TiO_2–$SrCo_{0.8}Fe_{0.2}O_3$ membranes is illustrated in Figs. 9 and 10, respectively. Both figures indicate that as the temperature increased, the O_2 and N_2 permeances decreased. Fig. 9 demonstrates that O_2 exhibited a higher permeance compared to N_2. However, both the O_2 and N_2 permeances decreased as the operating temperature increased from 28 to 350 °C. As the temperature increased, the permeance of O_2 decreased from 3.29E-06 to 1.08E-06 mol/m^2 Pa s (67.1% drop); the permeance of N_2 decreased from 2.83E-06 to 1.07E-06 mol/m^2 Pa s (62.2% drop). The decreased permeances were mainly due to a gradual reduction in surface diffusion. Generally, the loading factor and surface diffusivity will decrease at higher temperatures [23]. This trend is similar to that observed for Al_2O_3–SiO_2 membranes and indicates that the decrease in O_2 and N_2 permeance as a function of temperature was due to the lower apparent activation energy [24].

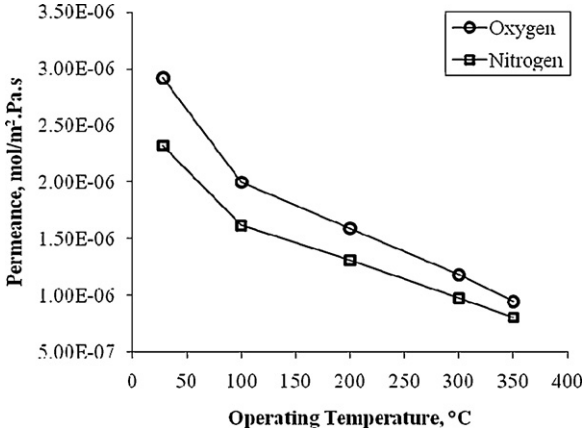

Fig. 10. Permeance of O_2 and N_2 across TiO_2–$SrCo_{0.8}Fe_{0.2}O_3$ membrane as a function of the operating temperature.

The permeation results for the TiO_2–$SrCo_{0.8}Fe_{0.2}O_3$ membrane show a similar trend to the TiO_2 membrane. As seen in Fig. 10, the O_2 permeance decreased from 2.92E-06 to 9.49E-07 mol/m^2 Pa s (a 67.5% drop), while the N_2 permeance dropped from 2.32E-06 to 8.08E-07 mol/m^2 Pa s (a 65.2% drop). The decrease of permeance at higher temperatures was a consequence of improved surface exchange caused by the addition of $SrCo_{0.8}Fe_{0.2}O_3$. The effect on O_2 permeance is more apparent at lower temperatures. The same trend was previously reported using a Ag-doped $SrCo_{0.8}Fe_{0.2}O_{3-\delta}$ oxide membrane [25].

The O_2 exhibits a higher permeance, compared to N_2, for both of the membranes because the order of permeance rates for gases follows the order of kinetic diameters. The kinetic diameter of N_2 (3.64 Å) is larger than that of O_2 (3.46 Å) [26].

Fig. 11 shows O_2/N_2 selectivity as a function of the operating temperature for TiO_2 and TiO_2–$SrCo_{0.8}Fe_{0.2}O_3$ membranes. It shows that the selectivity for both of the membranes decreased as the operating temperature increased. The TiO_2–$SrCo_{0.8}Fe_{0.2}O_3$ membrane shows the highest O_2/N_2 selectivity (1.26) at 28 °C, while the TiO_2 membrane possesses the lowest O_2/N_2 selectivity at 350 °C (1.01). The transport mechanism of the O_2/N_2 selectivity for both membranes predominantly involves the Knudsen diffusion mechanism because the value approaches the theoretical O_2/N_2 selectivity for the Knudsen diffusion mechanism (1.07), which is defined as the square root of the ratio of the heavier molecular weight gas (O_2) to the lighter molecular weight gas (N_2).

The trend for TiO_2 membrane selectivity indicates that the gas permeates mostly through the pores formed in the

crystalline TiO_2 membrane [27]. The observations indicate that the addition of $SrCo_{0.8}Fe_{0.2}O_3$ successfully increased the O_2/N_2 selectivity and, at the same time, the ability of the membrane to separate O_2 from N_2. In addition, the increase in O_2/N_2 selectivity implies that the large pore size in the TiO_2 membrane was successfully filled with $SrCo_{0.8}Fe_{0.2}O_3$. $SrCo_{0.8}Fe_{0.2}O_3$ contains several transition metal oxides (Fe and Co) that have been reported to be high-temperature adsorbents for gas separation. In addition, they theoretically have an infinitely high selectivity for O_2 over N_2 or other non-O_2 species [28].

4. Conclusion

TiO_2 membranes containing $SrCo_{0.8}Fe_{0.2}O_3$ were successfully prepared by the sol–gel method in combination with a wet impregnation process. Based on our findings, the optimal peptization ratio of H^+/Ti^{4+} was found to be 0.5, which results in the formation of a stable and deflocculated sol with TiO_2 fully in the anatase phase. The optimal calcination temperature for TiO_2 and $SrCo_{0.8}Fe_{0.2}O_3$ was 400 °C. At this temperature, TiO_2 is fully transformed to the anatase phase, while the PVA and HPC are completely removed, and the oxidation process of $SrCo_{0.8}Fe_{0.2}O_3$ is complete. A single coating of the TiO_2 membrane on the membrane support resulted in cracks and an uneven surface because of the quality of the surface on which the membrane was formed. A crack-free and homogeneous surface of the TiO_2–$SrCo_{0.8}Fe_{0.2}O_3$ membrane was obtained after multiple dip-coatings of the TiO_2 membrane, followed by a $SrCo_{0.8}Fe_{0.2}O_3$ wet impregnation process. While examining TiO_2–$SrCo_{0.8}Fe_{0.2}O_3$ membrane performance, it was found that addition of $SrCo_{0.8}Fe_{0.2}O_3$ to the TiO_2 membrane, which acts as a filler phase, successfully increased the O_2/N_2 selectivity of the TiO_2 membrane. The highest selectivity of TiO_2–$SrCo_{0.8}Fe_{0.2}O_3$ membrane was 1.26, compared to 1.16 for the TiO_2 membrane. Therefore, it can be concluded that the TiO_2–$SrCo_{0.8}Fe_{0.2}O_3$ membrane prepared using the described method has great potential in applications such as the separation of O_2 and as an O_2 enrichment membrane.

Acknowledgements

The authors gratefully acknowledge the research funding provided by the Universiti Sains Malaysia through the Fundamental Research Grant Scheme (FRGS) and a short-term research grant. The authors also acknowledge Dr. Mohd Azmier Ahmad for providing the membrane permeation test rig. Nur Aimie acknowledges the USM Fellowship for the support of her studies.

References

[1] Y.S. Lin, A.J. Burggraaf, Preparation and characterization of high temperature thermally stable alumina composite membrane, J. Am. Ceram. Soc. 74 (1991) 219–224.

[2] S.P.S. Badwal, F.T. Chiacchi, Ceramic membrane technologies for oxygen separation, Adv. Mater. 13 (2001) 993–996.

[3] T.V. Gestel, C. Vandecasteele, A. Buekenhoudt, C. Dotremont, J. Luyten, R. Leysen, B. Van der Bruggen, G. Maes, Alumina and titania multilayer membranes for nanofiltration: preparation, characterization and chemical stability, J. Membr. Sci. 207 (2002) 73–89.

[4] M.R. Mohammadi, M.C. Cordero-Cabrera, D.J. Fray, M. Ghorbani, Preparation of high surface area titania (TiO_2) films and powders using particulate sol–gel route aided polymeric fugitive agents, Sens. Actuators B: Chem. 120 (2006) 86–95.

[5] M.R. Mohammadi, D.J. Fray, M.C. Cordero-Cabrera, Sensor performance of nanostructured TiO_2 thin films derived from particulate sol–gel route and polymeric fugitive agents, Sens. Actuators B: Chem. 124 (2007) 74–83.

[6] S. Liu, K. Li, Preparation TiO_2/AI_2O_3 composite hollow fibre membranes, J. Membr. Sci. 218 (2003) 269–277.

[7] B.L. Bischoff, M.A. Anderson, Peptization process in the sol–gel preparation of porous anatase (TiO_2), Chem. Mater. 7 (1995) 1772–1778.

[8] M. Gopal, W.J.M. Chan, L.C. de Jonghe, Room temperature synthesis of crystalline metal oxides, J. Mater. Sci. 32 (1997) 6000–6008.

[9] M.C. Cordero-Cabrera, G.S. Walker, D.M. Grant, Effect of processing parameters on the particle size and stabilisation of titania sols, J. Mater. Sci. 40 (2005) 3709–3714.

[10] M.R. Mohammadi, D.J. Fray, A. Mohammadi, Sol–gel nanostructured titanium dioxide: controlling the crystal structure, crystallite size, phase transformation, packing and ordering, Microporous Mesoporous Mater. 112 (2008) 392–402.

[11] J. Tong, W. Yang, R. Cai, B. Zhu, L. Lin, Titanium-base perovskite-type mixed conducting ceramic membranes for oxygen permeation, Mater. Lett. 56 (2002) 958–962.

[12] G. Etchegoyen, T. Chartier, P. Del-Gallo, An architectural approach to the oxygen permeability of a $La_{0.6}Sr_{0.4}Fe_{0.9}Ga_{0.1}O_{3-\delta}$ perovskite membrane, J. Eur. Ceram. Soc. 26 (2006) 2807–2815.

[13] A.L. Ahmad, N.F. Idrus, M.R. Othman, Preparation of perovskite alumina ceramic membrane using sol–gel method, J. Membr. Sci. 262 (2005) 129–137.

[14] K. Li, Ceramic Membrane for Separation and Reactions, John Wiley & Sons Ltd, England, 2007.

[15] V.T. Zaspalis, W. Van Praag, K. Keizer, J.R.H. Ross, A.J. Burggraaf, Synthesis and characterization of primary alumina, titania and binary membranes, J. Mater. Sci. 27 (1992) 1023–1035.

[16] A. Alem, H. Sarpoolaky, M. Keshmiri, Titania ultrafiltration membrane: preparation, characterization and photocatalytic activity, J. Euro. Ceram. Soc. 29 (2009) 629–635.

[17] V.N. Koparde, P.T. Cummings, Phase transformations during sintering of titania nanoparticles, ACS Nano 2 (8) (2008) 1620–1624.

[18] S. Winardi, R.R. Mukti, K.N.P. Kumar, J. Wang, W. Wunderlich, T. Okubo, Critical nuclei size, initial particle size and packing effect on the phase stability of sol-peptization–gel-derived nanostructured titania, Langmuir 26 (7) (2010) 4567–4571.

[19] D.S Bae, K.S. Han, S.H. Choi, Preparation and thermal stability of doped TiO_2 composite membranes by the sol–gel process, Solid States Ionics 109 (1998) 239–245.

[20] W. Chen, J. Zhang, Q. Fang, S. Li, J. Wu, F. Li, K. Jiang, Sol–gel preparation of thick titania coatings aided by organic binder materials, Sens. Actuators B: Chem. 100 (2004) 195–199.

[21] N. Agoudjil, T. Benkacem, Synthesis of porous titanium dioxide membranes, J. Desalinat. 206 (2007) 531–537.

[22] M.R. Mohammadi, D.J. Fray, Low-temperature perovskite-type cadmium titante thin films derived from a simple particulate sol–gel process, Acta Mater. 57 (2009) 1049–1059.

[23] A.L. Ahmad, M.R. Othman, H. Mukhtar, H_2 separation from binary gas mixture using coated alumina–titania membrane by sol–gel technique at high-temperature region, Int. J. Hydrogen Energy 29 (2004) 817–828.

[24] R.S.A. De Lange, J.H.A. Hekkink, K. Keizer, A.J. Burggraaf, Permeation and separation studies on microporous sol–gel modified ceramic membranes, Micro. Mater. 4 (1995) 169–186.

[25] L. Tan, L. Yang, X. Gu, W. Jin, L. Zhang, N. Xu, Structure and oxygen permeability of Ag-doped $SrCo_{0.8}Fe_{0.2}O_{3-\delta}$ oxide, Am. Inst. Chem. Eng. 50 (3) (2004) 701–707.

[26] T.D. Kusworo, A.F. Ismail, A. Mustafa, Budiyoni, Application of activated carbon mixed matrix membrane for oxygen purification, Int. J. Sci. Eng. 1 (1) (2010) 21–24.

[27] H.Y. Ha, S.W. Nam, T.H. Lim, I.H. Oh, S.A. Hong, Properties of the TiO_2 membranes prepared by CVD of titanium tetraisopropoxide, J. Membr. Sci. 111 (1996) 81–92.

[28] H. Hao, L. Zhao, J. Hu, X. Hu, H. Hou, Oxygen adsorption/desorption behavior of $YBaCo_4O_{7+\delta}$ and its application to oxygen removal from nitrogen, J. Rare Earth 27 (5) (2009) 815–818.